Comparing spatial metrics of extreme precipitation between data from rain gauges, weather radar and high-resolution climate model re-analyses

Thomassen, Emma Dybro; Thorndahl, Søren Liedtke; Andersen, Christoffer Bang; Gregersen, Ida Bülow; Arnbjerg-Nielsen, Karsten; Sørup, Hjalte Jomo Danielsen

Published in:
Journal of Hydrology

DOI (link to publication from Publisher):
10.1016/j.jhydrol.2022.127915

Publication date:
2022

Document Version
Publisher's PDF, also known as Version of record

Journal of Hydrology 610 (2022) 127915

Contents lists available at ScienceDirect

Journal of Hydrology

journal homepage: www.elsevier.com/locate/jhydrol

Research papers

Comparing spatial metrics of extreme precipitation between data from rain gauges, weather radar and high-resolution climate model re-analyses

Emma Dybro Thomassen [a,b], Søren Liedtke Thorndahl [c], Christoffer Bang Andersen [c], Ida Bülow Gregersen [d], Karsten Arnbjerg-Nielsen [a], Hjalte Jomo Danielsen Sørup [a,*]

[a] Technical University of Denmark, Department of Environmental and Resource Engineering, Climate and Monitoring, Lyngby, Denmark
[b] Danish Meteorological Institute, National Center for Climate Research, Copenhagen, Denmark
[c] Aalborg University, Department of the Built Environment, Aalborg, Denmark
[d] Rambøll Denmark A/S, Department of Climate Adaptation and Green Infrastructure, Copenhagen, Denmark

ARTICLE INFO

This manuscript was handled by Andras Bardossy, Editor-in-Chief

Keywords:
Convective permitting model
e-folding distance
ERA-Interim
Intensity-duration frequency curves
Regional climate model
Spatial correlation
Weather radar

ABSTRACT

The representation of extreme precipitation at small spatio-temporal scales is of major importance in urban hydrology. The present study compares point and radar observations to reanalyse climate model output data for a period of 14 years where there is full spatial and temporal overlap between datasets. The datasets are compared with respect to seasonality of occurrence, intensity levels and spatial structure of the extreme events. All datasets have similar seasonal distributions and comparable intensity levels. There are, however, clear differences in the spatial correlation structure of the extremes. Seemingly, the radar data is the best representation of a "real" spatial structure for extreme precipitation, even though challenges appear in data when moving far from the physical radar. The spatial correlation in point observations is a valid representation of the spatial structure of extreme precipitation. The convective-permitting climate model seems to represent the spatial structure of extreme precipitation much more realistically, compared to the coarser convective parameterized model. However, there is still room for improvement of the convective-permitting climate model for the shortest rainfall durations and smallest spatial scales in comparison with point and radar data.

1. Introduction

Many hydrological studies use standardized precipitation data with daily resolution and decadal kilometre spatial scales for hydrological impact analyses, e.g. Refsgaard (1997) and Karlsson et al. (2016). This has led to the construction of large reanalysis datasets (Cornes et al., 2018), that are generally used for many impact studies. However, as pointed out by e.g. Berne et al. (2004) and Ochoa-Rodriguez et al. (2015) urban hydrology applications, in general, require a much higher spatio-temporal description of extreme statistics of precipitation, due to the short response time in urban water systems. Understanding and describing the properties of precipitation in sub-hourly and square kilometre scales remains a challenge, not only when assessing climate change impacts, but also for the description of the current climate (Arnbjerg-Nielsen et al., 2013; Thorndahl et al., 2017). A key issue is that the precipitation-generating mechanism changes when moving from large-scale to urban scale, from primarily being driven by frontal movement and orographic effects to the relatively infrequent, but important, convective storms at urban scale (Ban et al., 2021). This leads to substantial differences in spatial correlation distances, ranging from less than 10 km on precipitation events with durations of 10 min to several hundreds of kilometres on daily data (Madsen et al., 2002).

The analysis of spatial metrics serves multiple specific purposes related to urban hydrology. In regional extreme value statistics of rainfall based on point statistics (e.g. Gregersen et al., 2017; Madsen et al., 2017) the spatial correlation is applied to certify statistical independence between stations. In statistical downscaling of regional climate models (RCMs) (e.g. Willems and Vrac, 2011) the spatial structures are important to derive climate indices at the spatial and temporal scale of the application in question. In application and comparison of spatio-temporal rainfall data of different resolutions (e.g. high-resolution RCM data or radar data) as inputs to hydrological models (e.g. Ochoa-Rodriguez et al., 2015; Thorndahl et al., 2016). In the design of urban hydrological systems, the spatial scale is of importance, e.g. in the use of areal reduction factors (Rosbjerg and Madsen, 2019; Thorndahl et al., 2019; Vaes et al., 2005).

* Corresponding author.
E-mail address: hjds@dtu.dk (H.J.D. Sørup).

https://doi.org/10.1016/j.jhydrol.2022.127915
Received 10 November 2021; Received in revised form 29 April 2022; Accepted 3 May 2022
Available online 9 May 2022

During the past decade, there has been much attention to the accuracy of RCMs with respect to the representation of high-resolution extreme precipitation. As part of this attention, several new metrics have been developed and applied with a focus on spatial correlation as a function of the temporal resolution (Gregersen et al., 2013; Mayer et al., 2015; Sørup et al., 2016; Sunyer et al., 2013). Gregersen et al. (2013) pointed out that the spatial correlation structures observed in the ENSEMBLES climate data were very different from the one observed in point observations. Mayer et al., (2015) compared point measurements to climate model data with higher resolution and showed a decreasing error in spatial correlation of extreme precipitation with higher resolution of the climate models. The analysis was performed on climate models with resolutions from 8 to 70 km and also compared to point observations. Both Gregersen et al. (2013) and Mayer et al., (2015) base their analysis on climate models constructed with a parametrization scheme for convective rainfall, while high-resolution convective permitting climate models (CPMs) have gained attention more recently (Kendon et al., 2014), also for Scandinavia (Lind et al., 2020; Olsson et al., 2021). To the knowledge of the authors, the spatial correlation of extreme precipitation has not been explicitly assessed for the new CPMs. However, Thomassen et al., (2021) showed how the general structure of extreme precipitation in these high-resolution models is indeed very different compared to the coarser resolution parameterized ones.

Radar data is often compared to point observations for verification and bias correction purposes (Schleiss et al., 2020; Thorndahl et al., 2017) and there are examples of studies where the spatial correlation structure of extremes in radar data is studied (e.g., Thomassen et al., 2020) and compared to point measurements (e.g., Thorndahl et al., 2019). Radar data has also recently been used as a basis for downscaling of re-analysis products to finer, urban relevant, scales (Emmanouil et al., 2021).

In the present study, we calculate different spatial and temporal metrics for extreme precipitation and compare point observations, radar precipitation and high-resolution RCM re-analysis data for the same region and period. Extreme precipitation events are defined for each duration from the series of event based maximum intensities by including intensities above a pre-defined threshold level corresponding to approximately three events per year in accordance with previous studies using the same data (Madsen et al., 2017). This enables a systematic evaluation of accuracy with respect to the magnitudes and annual variations of the extremes, as well as the spatial correlation patterns for different temporal resolutions. In particular, the aim is to:

1) validate the metrics between point rainfall and radar products and identify if and how much extra information radar data provide compared to the point observation dataset with respect to the spatial extent of extreme events, and
2) assess how well high-resolution RCMs are able to model this observed spatial behaviour of extreme precipitation events.

2. Data and methods

2.1. Data

This study compares observational point measurements from tipping bucket rain (POINT), bias-corrected records from a weather radar (RADAR), and reanalysis data from two high-resolution regional climate models, one being a traditional RCM while the other is a CPM. Only data covering the same spatial and temporal domain is included in the analysis to ensure full comparability, leading to analysis of datasets of 14 years duration (2005 to 2018) on a spatial domain of land cells in south-eastern Denmark approximately 120 km (lat) by 175 km (lon) (Fig. 1). Both the RADAR and the RCM models have extensive periods

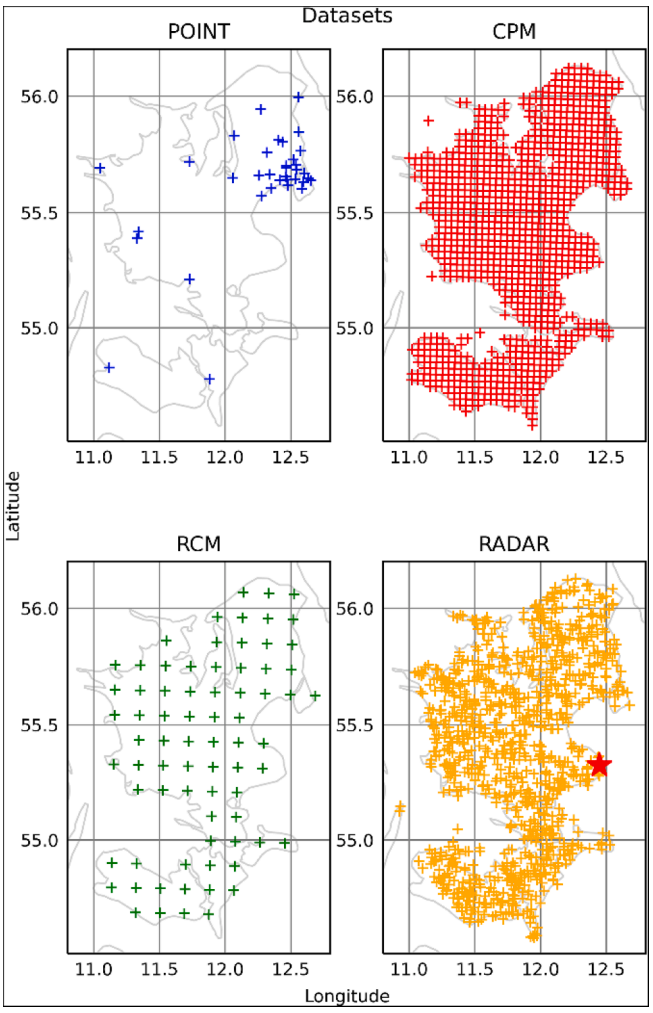

Fig. 1. Spatial distribution of data points in the south-eastern part of Denmark (Zealand and southern islands) from the four datasets included in the analysis; tipping bucket rain gauge (POINT – blue), CPM at 3 km resolution (CPM – red), RCM at 12 km resolution (RCM – green) and bias-corrected weather radar (RADAR – yellow). The crosses mark the locations of the gauges or grid points used from each of the individual datasets in the analysis. The red star in the RADAR data set marks the location of the radar (near Copenhagen). (For interpretation of the references to colour in this figure legend, the reader is referred to the web version of this article.)

with very low precipitation intensities, known as drizzle, that lead to an unreasonable distribution between wet and dry periods as well as prohibits an easy separation into precipitation events. Therefore, drizzle thresholds are applied to this data in the analysis as outlined below. This way all data products have around 200 precipitation events per year at each data point. From these events the extreme events are selected, assuming an independence criterion based on dry weather periods (Madsen et al., 2017). The area is rather homogeneous with respect to precipitation, with mean annual precipitation ranging from 550 to 750 mm. The landscape is flat and homogeneous compared to international standards, with altitudes ranging from 0 to 120 m above sea level.

The POINT data have a resolution of 0.2 mm and 1 min and are from The Water Pollution Committee of The Society of Danish Engineers rain gauge network (Gregersen et al., 2013; Madsen et al., 2017). For the defined spatial and temporal domain there are 34 stations with full data coverage used for this study. The quality control is outlined in Jørgensen

et al., (1998) and only shorter periods of data are missing from individual gauges in the period. Despite the uneven clustering of POINT data (Fig. 1), this dataset is used in the common Danish dimensioning practice for urban sewer systems by applying a regional model as outlined in Madsen et al. (2017).

The RADAR data is based on a single C-band radar located at Stevns (approximately 50 km south of Copenhagen) operated by the Danish Meteorological Institute (DMI). The radar data is remapped from a polar to a Cartesian grid in a 500 m by 500 m resolution and in this study limited to a range of 100 km from the location of the radar. Due to the radar's beamwidth and angular resolution of 1 degree, and gated range bins of 500 m, a true 500 m by 500 m resolution is only valid until a range of approximately 30 km from the radar. The radar data is therefore slightly oversampled in azimuth in ranges from 30 to 100 km. Based on the volume scans consisting of nine elevation scans (0.5 degree to 15 degree) a pseudo-CAPPI product is generated at a fixed altitude of 1 km. The rainfall product is therefore a composite of multiple elevations scans up to a range of approximately 70 km. In ranges larger than 70 km the lowest elevation scan (0.5 degree) is applied and the radar observations, therefore, exceeds the 1 km altitude. The temporal sampling is performed in 10-minute intervals. An advection interpolation procedure applying the method described in Nielsen et al. (2014) transforms the data to a temporal resolution of 1 min. The dataset is quality controlled and mean-field bias-adjusted on daily rain gauge data using the method described in Thorndahl et al. (2014). A total of 96 rain gauge stations is used for the bias adjustment. These stations have a heterogeneity in the spatial distribution and more rain gauge stations are available in the last part of the data period than in the first part. However Thorndahl et al. (2014) argue that this is of minor importance for the overall mean-field-bias adjustment in analysing events with daily rainfall>5 mm as is the case in this study. The same radar data has been evaluated with regard to the estimation of heavy rainfall in Schleiss et al. (2020). A drizzle threshold of 0.1 mm/hr is applied and rain intensities below this threshold are considered as no rain. Section 3.4 provides a detailed discussion on how the nature of radar data (such as range and elevation) and data processing affects the precision of estimated rainfall intensities and derived spatial correlation metrics. In this study, the data set is limited to 1500 randomly selected cells within the selected domain (Fig. 1, RADAR). Rather than selecting cells by a structured grid resampling, we apply random sampling to ensure neighbouring and close proximity cells to be included in the spatial correlation analysis.

Both reanalysis datasets (RCM and CPM) are based on the Harmonie Climate model system, HCLIM cycle 38 (Belušić et al., 2020) using two different physics packages, which allows completely different model data to be created with the same overall model system: ALADIN (RCM) and AROME (CPM) (Termonia et al., 2018). RCM has a 12 km spatial and one-hour temporal resolution with a convective parameterization scheme. CPM is "convective-permitting" with only shallow convection being parameterized while deep convection is non-parametrized due to the grid size. CPM has a 3 km spatial and 15-minute temporal resolution (Lind et al., 2020). In this study reanalysis model output data driven by ERA-Interim is used (Dee et al., 2011). RCM is directly downscaled from ERA-Interim, while CPM is downscaled from RCM and is hence double nested. Model data is available in a Fenno-Scandinavian domain (Lind et al., 2020) and data points within the study area are selected based on a land-sea fraction above 40%. A drizzle threshold of 0.2 mm/hr is applied to both model datasets, considering intensities below this threshold dry.

2.2. Methods

2.2.1. Sampling of extreme events

For each data record, the most extreme events are sampled using a Peak Over Threshold method with a flexible threshold resulting in 3 events per year on average (Gregersen et al., 2013; Madsen et al., 2002). Each station and grid point is sampled individually resulting in the same number of events per year for each sampling point. This way results are comparable across different data types (Gregersen et al., 2013; Mayer et al., 2015).

Individual event intensities are sampled for eight rainfall durations between 15 min and 48 h (15, 30, 60, 180, 360, 720, 1440 and 2880 min). Events are considered independent if there is a dry period between them of at least the same length as the rainfall duration considered; i.e. for 1440 min extremes, individual events have to be separated by at least 1440 min of dry weather, this is in accordance with previous studies (e.g. Gregersen et al., 2013; Madsen et al., 2009; Madsen et al., 2002).

2.2.2. Magnitude and seasonal variation of extreme events

The magnitude of the extreme events is compared between the four datasets (POINT, RADAR, RCM and CPM) by a simple calculation of intensities for relevant return periods. As the different datasets represent the same actual observed weather, the full record length is used for this with the return period, T, calculated using the median plotting position:

$$T = \frac{N + 0.4}{rank - 0.3} \tag{1}$$

where N is the length of the time series and *rank* is the rank of the extreme event.

The seasonality of the extremes is determined by a division of the sampled extreme events based on their season of occurrence. This allows for a determination as to whether the sampled extremes follow the same seasonal pattern in the different datasets.

2.2.3. Unconditional spatial correlation of extreme events

The unconditional spatial correlation, ρ, is determined for all datasets based on the methodology of Mikkelsen et al., (1996). This measure describes the concurrence of extremes for any given duration, and is, hence, often interpreted as the spatial correlation of the meteorological phenomena. The unconditional spatial correlation measure was first derived in Mikkelsen et al. (1996), but here a shorter presentation is given, based on the description in Gregersen et al. (2013).

The first step is to pair events for the two separate locations, denoted A and B, respectively. A stochastic variable U is defined and given the value of 1 if the two events are concurrent, and 0 if they are not. Concurrency is defined by considering a time window (or lag time) relative to the start time of each of the exceedances. If there is an exceedance at the other station within this lag time U takes the value of 1, and 0 otherwise. Both Mikkelsen et al (1996) and Gregersen et al (2013) apply a lag time of 11 h. Since the effect of the lag time length has not been tested in previous studies, we investigate the effect of different maximum lag times between 0 and 48 h in the POINT dataset.

The second step is then to calculate the unconditional covariance, accounting also for extreme events at the two sites that are not concurrent. Mikkelsen et al (1996) show that this corresponds to calculating the correlation between the mean values of the exceedances, Z_A and Z_B, respectively, and derives the following equation for this covariance:

$$Cov\{Z_A, Z_B\} = Cov\{E\{Z_A|U\}, E\{Z_B|U\}\} + E\{Cov\{Z_A, Z_B|U\}\} \tag{2}$$

Finally, the correlation of extremes between two observation points is calculated by dividing the covariance of the extremes with the product of the sampling standard error, σ_A and σ_B at these points:

$$\rho_{AB} = \frac{Cov(Z_A, Z_B)}{\sigma_A \sigma_B} \tag{3}$$

The correlation is aggregated in bins of similar distances and is assumed to decay exponentially as a function of spatial distance. We use bins for every 10 km distance for this study, where for each the mean

correlation and distance is determined. Based on these results and the number of individual correlation pairs in each bin, we fit a two-parameter exponential function:

$$\rho = e^{\left(-\frac{d^{\alpha}}{\beta}\right)} \quad (4)$$

The two parameters, α and β, are necessary in order to secure full correlation at distance d = 0 km. Finally, we compute the *e*-folding distance based on these exponential functions; i.e. the distance by which the correlation is decreased to $\rho = 0.37$ of the initial correlation (e.g. Ha et al., 2007). This simple metric enables a simple comparison between different durations and data products and compared to the sampling uncertainty gives a sufficiently accurate description of the spatial correlation.

3. Results and discussion

3.1. Magnitude of extreme rainfall intensities

The simple comparison of intensity distributions for extremes for different return levels between the four datasets indicates substantial differences (Fig. 2). The coarser climate model data (RCM) clearly have lower intensities across all scales and return periods. This is following the conclusions of previous studies (Gregersen et al., 2013; Mayer et al., 2015; Vaes et al., 2005). The high-resolution climate model data (CPM) on the other hand shows intensities very close to the ones observed for both point observations (POINT) and radar (RADAR) data. This supports previous studies showing how rainfall in these types of models overall behave more like observations compared to coarser models (Médus et al., 2022; Olsson et al., 2021; Thomassen et al., 2021). The RADAR, CPM, and RCM results all indicate a tendency towards a flattening of the IDF-curve for short durations, most likely due to the spatial representation of these datasets versus the POINT observations. This scaling error between point and area has been documented by many authors (Ciach and Krajewski, 1999; Peleg et al., 2018; Thorndahl et al., 2019; Wang et al., 2015). Thorndahl et al. (2019) implement a simple duration-dependent bias correction, to overcome the problem, but in the spatial analysis (section 3.3), such a correction will have no effect. This is due to the fact that the estimated spatial correlations are based on relative measures for each duration and return period, and therefore independent of the magnitude of the rainfall intensities. It could, however, be relevant to include the bias correction, if a relationship between rainfall duration and spatial correlation should be established, but this is beyond the scope of the present paper.

From Fig. 2 a larger variability of the intensity distributions (dashed lines) are found for the RADAR data and the CPM data in comparison with the two other datasets. A reason to explain this is not found in the data values itself, but rather in the inhomogeneity of data density for each dataset (POINT: 35 data points and RCM: 74 data points versus RADAR: 1500 data points and CPM 1074 data points).

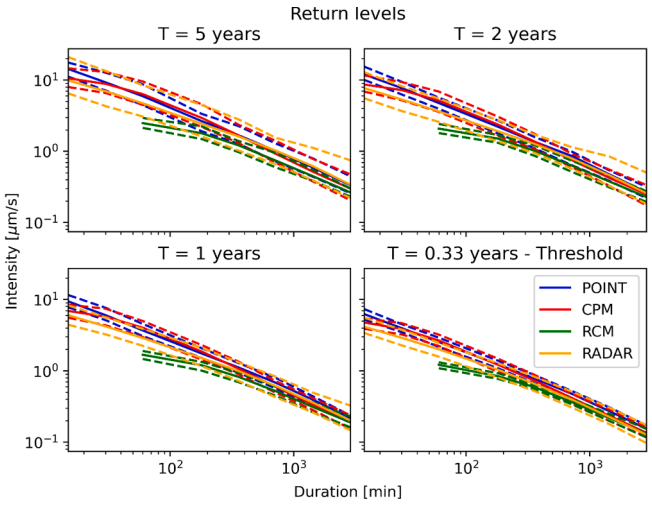

Fig. 2. Intensity distributions for the four datasets (POINT, RADAR, RCM and CPM) for different return periods. The dashed lines represent the min/max boundaries of all stations or grid points for each dataset (see Fig. 1), and thus represent the spatial variability.

3.2. Seasonality of extremes

The seasonal distribution between the sampled extreme events is very similar between the four datasets across all event durations (Fig. 3). This is expected because the analysis is based on observations and reanalysis of the same years. The resolution and data density does not seem to influence the seasonal distribution significantly. As expected, short-duration extreme events include a very large fraction of summer events, and even though the fractions drops for longer duration events, summer events remain the major fraction across all durations. For durations of 12 h or more, the fall season also starts to contribute a larger fraction of the extreme events, while the winter and spring seasons have low occurrences of extremes for all durations and datasets. In a prior study of coarser scale climate model reanalysis (Sunyer et al., 2013), the seasonal distribution of extreme rainfall intensities is more uniform. Since, in this case, the RCM model shows the same tendency in seasonal distribution as the other higher-resolution datasets, the confidence in the RCM model's ability to simulate extreme rainfall and inter-seasonal changes is strengthened.

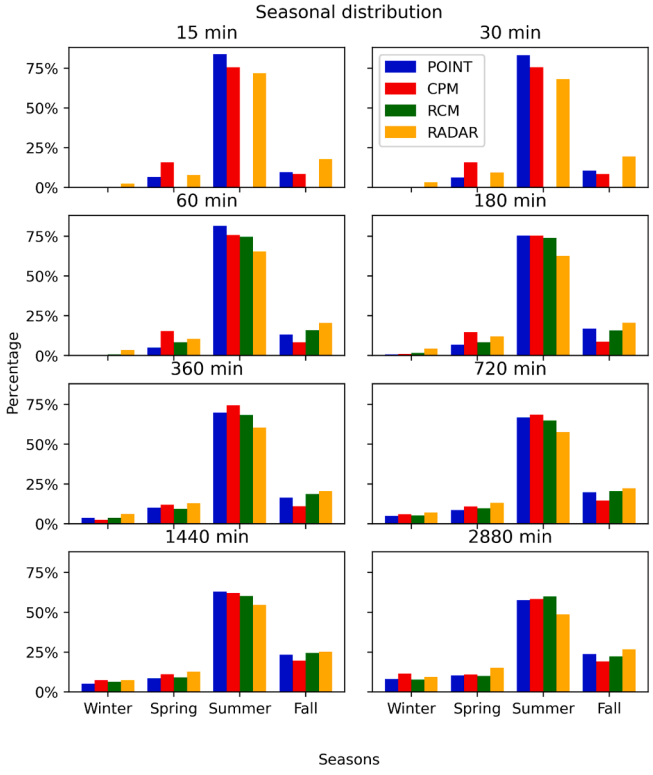

Fig. 3. Seasonal distribution of sampled extreme events for the four datasets (POINT, RADAR, RCM and CPM). Extreme events are sampled by the maximum intensity for durations ranging between 15 and 2880 min. For each duration, the percentages for each dataset equals 100% across all seasons.

3.3. Unconditional spatial correlation

As described in section 2.2.3, the correlation is calculated for each pair of gauges/grid point for each dataset and duration, these are binned according to distance between the gauges/grid points, and an exponential function is fitted in order to describe the correlation and calculate the e-folding distance. Fig. 4 illustrate this process for the POINT dataset for a duration of 1440 min. In the remainder, we will only report the fitted functions and the e-folding distances.

First, we test the influence of lag time on the unconditional spatial correlation of the POINT dataset. The lag time is used to separate individual events in space and time. If the time between the end of an event at one location and the start of an event at another location, is less than the lag time, the event is considered to belong to the same storm system, and therefore, the events are paired and given the value $U = 1$, i.e. equation (2). On the other hand, if the time between the two events exceeds the lag time, they are considered belonging to two different storm systems and thus not paired, i.e. given a value of $U = 0$. The start and end times of the individual events are estimated from the moving average over the duration in question. For a continuous rain series, the point in time where the time-averaged intensity becomes zero marks the end of an event, and correspondingly the shift to a positive intensity marks the start of an event. For radar and climate model data, the time-averaged intensities below the drizzle threshold are given a value of zero.

The spatial correlation is calculated for different lag times between 0 and 48 h for durations between 15 and 2880 min for the POINT dataset (Fig. 5). The results show that only the lag time of 0 h is different from the other lag times and only for longer duration events. This means that only if there is a strict requirement of exact overlap in time of occurrence, it will have an impact on the calculated spatial correlation. All requirements allowing for some lag time between the points lead to the same estimates of spatial correlation. Hence, the lag time is concluded to be a parameter with less influence on the result, as long as the case area is as limited as in the present study.

The unconditional spatial correlations are subsequently calculated for all four datasets across the full range of durations using a lag time of 11 h in accordance with previous studies (Fig. 6). For durations between 15 and 1440 min, the results between POINT and RADAR are very similar (see also the e-folding distances in Table 1). Likewise, the results between RADAR and CPM are very similar between 360 and 2880 min. The RCM dataset seems to have generally higher correlations as a function of distance independent of the duration. This is most likely due

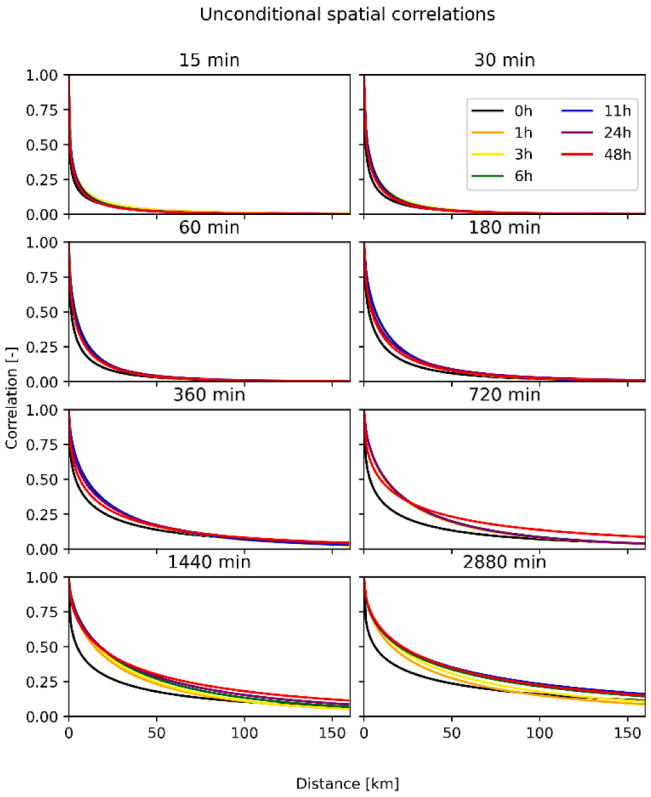

Fig. 5. Fitted unconditional spatial correlation for the POINT dataset for seven different lag times ranging from 0 to 48 h. The different unconditional spatial correlation curves visualise the sensitivity of the lag time parameter used to correlate events between stations.

to the RCM's parameterisation of convective rainfall (non-convective permitting) and is much in line with observations from previous studies which showed that coarser resolution data generally resulted in longer correlation distances (Gregersen et al., 2013; Mayer et al., 2015). The POINT dataset produces somewhat longer correlation distances for 2880 min events compared to RADAR and CPM. There can be two explanations for this. One likely explanation is that this is the result of the physical placement of rain gauges in POINT where there only exist very few possible pairs of gauges with +100 km distance separation. This

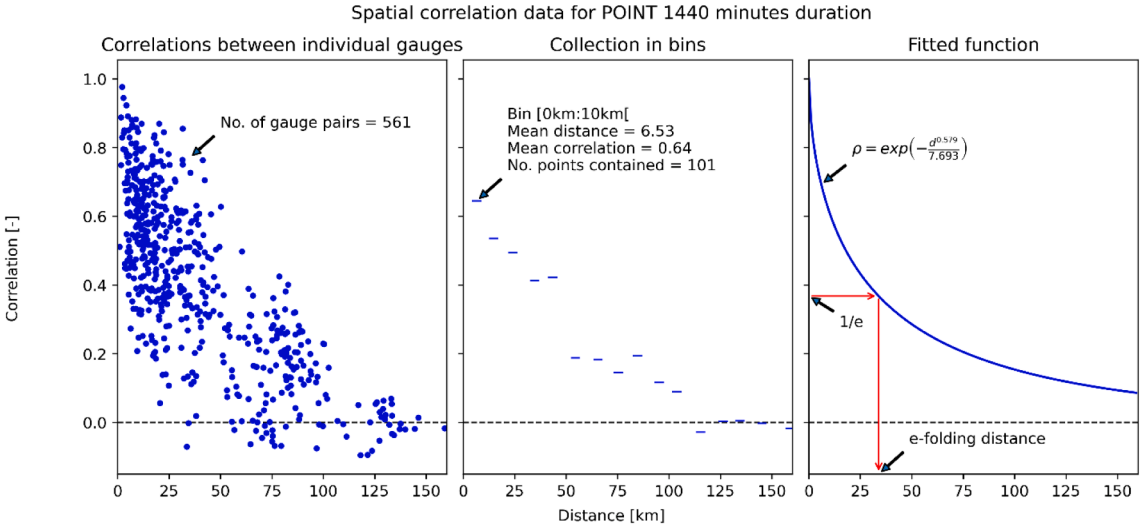

Fig. 4. Illustration of how 561 individually calculated spatial correlations between pairs of gauges (left) are transformed into correlation functions described by exponentials (right), using bins of 10 km (middle).

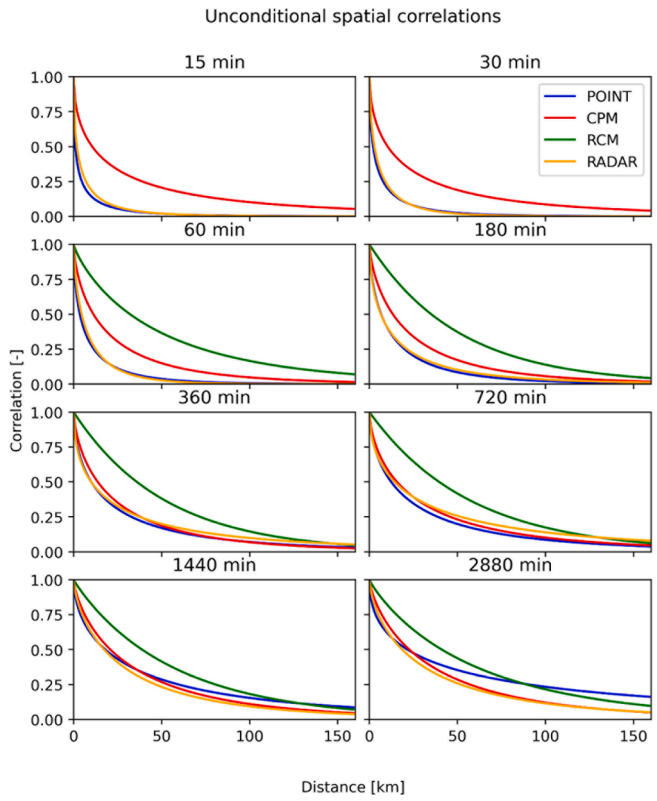

Fig. 6. The fitted unconditional spatial correlation for the four different datasets (POINT, RADAR, RCM and CPM). For RCM the correlation is only computed for 60 min and above due to the temporal resolution of this dataset. Extreme events are sampled by the maximum intensity for durations ranging between 15 (top left) to 2880 min (bottom right). A lag time of 11 h is used to correlate events between stations or grid points.

likely influences the result for these long-duration events, as they have to be measured as extremes in exactly these points compared to the high-resolution gridded datasets (RADAR and CPM) where the extreme "just" has to be measured somewhere at either end of the map to match in correlation. Another reason may be orographic impacts, since the precipitation gauges measure at ground level while the radar measures 1 km above ground where the orographic impacts are negligible, given the relatively moderate topography of the area. A previous study supports the second explanation (Gregersen et al 2013).

In general, the RADAR dataset shows a consistency of the correlations across all durations which indicates a good description of the actual rainfall behaviour and less impact of spatial and temporal resolution in comparison with CPM and RCM. The consistency across durations was also studied by Thorndahl et al. (2019) who developed a relationship between areal reduction factor (ARF) and duration based on radar data. Even though they derived areal reduction factors from a dataset with more events included and applied a storm-centred approach rather than an area-fixed approach (i.e. fixed locations, as applied in this study), the conversion from ARFs to e-folding distances shows very similar results (Table 1).

As described earlier, the RADAR dataset is influenced by the range from the physical radar location both in terms of the derived resolution as well as the altitude of observations in the atmosphere. In section 3.4 the range dependence is studied in more detail.

From Fig. 6 it is seen that the observed products (POINT and RADAR) are clearly the better of the four at describing the spatial structure of rainfall extremes at the sub-hourly to hourly time-scale. This is likely a combination of their superior spatial and temporal scales, which is much more likely to capture the detailed behaviour of convective storms. In contrast, the two re-analysis products (CPM and RCM) only start to perform well at temporal scales that are somewhat higher than their native time scales (15 and 60 min). For the CPM this occurs at the 60 to 360 min scales, whereas the RCM doesn't perform reasonably before the 1440 min scale. In contrast, the performance of the POINT datasets seems to decline for the longest duration (2880 min) where longer correlation distances are expected but these are poorly calculated due to very few pairs of gauges at long distances. Based on these observations, the corrected RADAR dataset seems to be the most consistent across scales, but the POINT dataset can be used when short durations and small spatial scales are considered, and, in contrast, the CPM seems very credible in situations where the sub-hourly scale is not of importance. The RCM preforms poorly at the accessed scales, but with its coarse resolution the dataset is never really applicable in urban hydrology.

3.4. *Subdivision of the RADAR dataset according to distance from the radar*

To test the influence of the procedures behind the RADAR pseudo-CAPPI product described in Section 2.1, the RADAR dataset is subdivided according to the distance from the radar. A threshold distance of 63 km is used as this results in two bins of almost equal sizes (754/746 grid points) and because this choice also enables a separation into a bin with a constant altitude and a bin with a gradually increasing altitude of the lower scans due to the Earths curvature (Fig. 7).

The two subdivisions have very similar intensity levels for the different return periods (Fig. 8) which is a result of the mean-field bias-adjustment of the dataset. In contrast to this, the spatial correlation between the two subdivisions is very different (Fig. 9, Table 1). The difference in spatial correlation between the POINT dataset and the RADAR observed for 2880 min duration using all RADAR grid points becomes more pronounced using only grid points in close proximity to the radar. Using only grid points close to the RADAR (<63 km), a shorter e-folding distance (Table 1) in the RADAR dataset compared to the POINT dataset, is found for durations above 720 min.

From the grid points far from the RADAR (>63 km) the correlation is significantly different with longer correlation distances above 360 min

Table 1
e-folding distances [km] for the four datasets (POINT, RADAR, RCM and CPM); also, (1) data from a previous calculation based on the POINT dataset for all of Denmark performed in Gregersen et al. (2013) is displayed and (2) data from splitting the RADAR dataset according to distance from the radar as discussed in the following section. The column RADAR-ARF (3) shows derived e-folding distances from a previous study on storm-centred areal reduction factors using the RADAR dataset (Thorndahl et al., 2019).

Duration	POINT	POINT-DK[1]	CPM	RCM	RADAR	<63 km RADAR[2]	> 63 km RADAR[2]	RADAR-ARF[3]
15 min	2		21		4	4	4	5
30 min	4		20		5	5	6	6
60 min	7	5	19	50	8	7	10	8
180 min	12	18	22	51	12	11	22	11
360 min	19		23	52	20	14	53	14
720 min	23	24	28	57	28	18	70	18
1440 min	34	37	34	57	29	24	49	23
2880 min	46		37	62	32	27	50	29

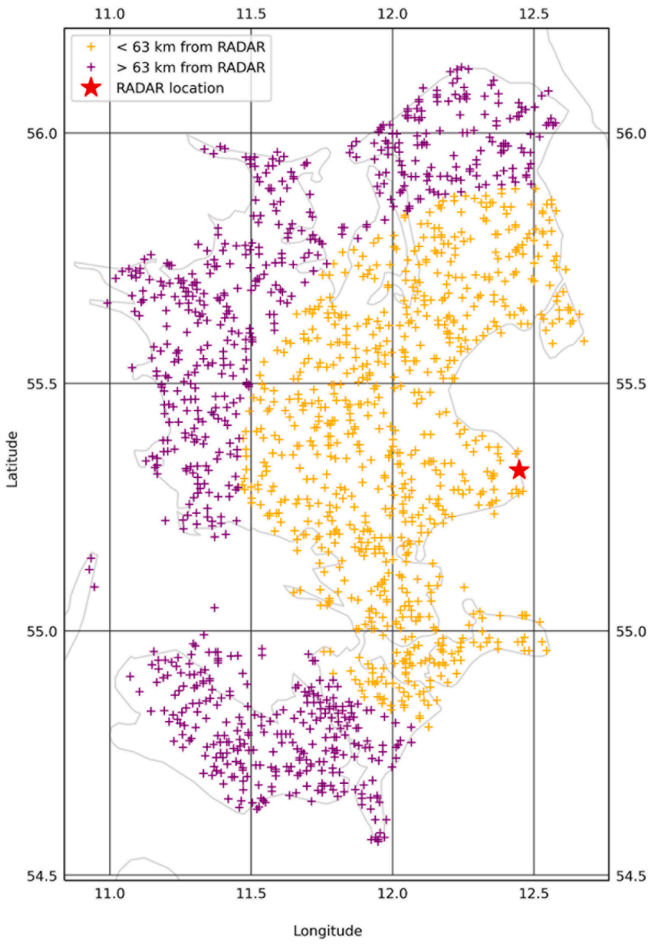

Fig. 7. Subdivision of the RADAR dataset according to distance to the radar. A distance of 63 km is used as division with a constant altitude within 63 km from the radar and increasing altitude beyond 63 km from the radar. The location of the radar (near Copenhagen) is marked with a star.

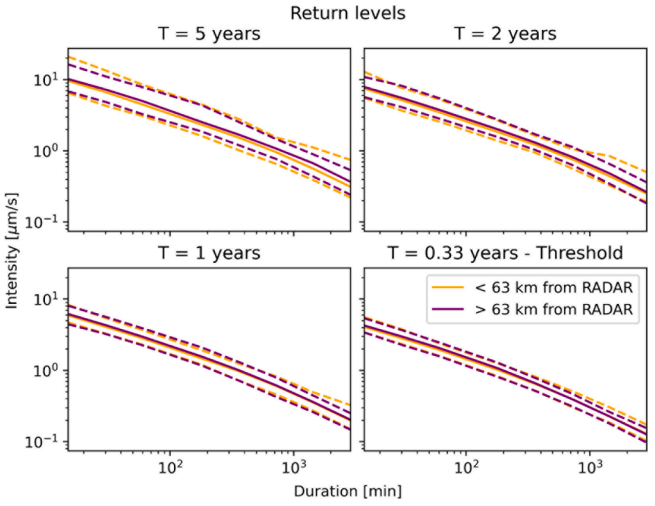

Fig. 8. Intensity distributions for the two subdivisions of the RADAR dataset (Fig. 7) for different return periods. Dotted lines represent the full spatial variability within each dataset.

(Fig. 9). The increase in radar beam elevation at larger ranges than 70 km, as an artefact of the pseudo-CAPPI construction, might result in larger correlations in higher elevations than closer to the ground. This

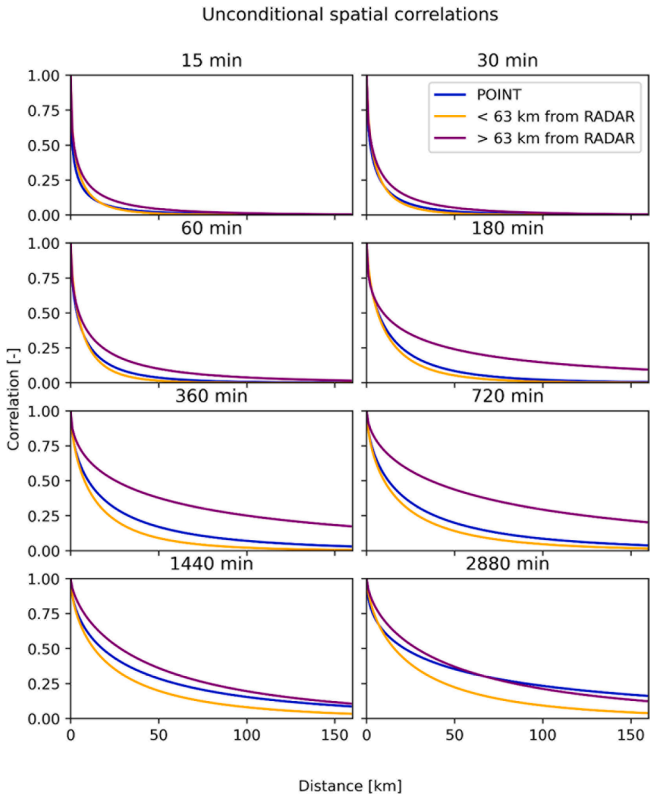

Fig. 9. Fitted unconditional correlations for the two different sub-sets of the RADAR dataset and the POINT dataset. Extreme events are sampled by the maximum intensity for durations ranging between 15 (top left) to 2880 min (bottom right). A lag time of 11 h is used to correlate events between stations or grid points.

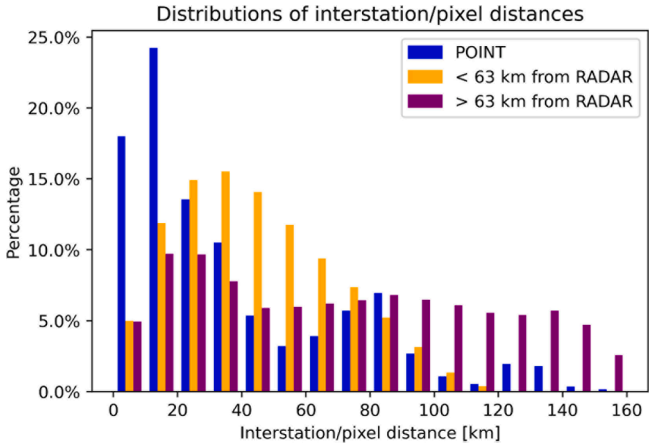

Fig. 10. Differences in the distribution of interstation/pixel distances between correlation pairs for the POINT dataset and the two subsets of the RADAR dataset, shown in Fig. 7. The percentages of each dataset equals 100% across all 10 km-bins.

might result in that it is the general frontal movements, which are captured rather than the actual measured rainfall at ground level.

Another explanation is the difference in the distribution of correlation pairs behind the e-folding estimation (Fig. 10). Where the POINT dataset is dominated by pairs of stations with short distances apart (<20 km) the RADAR data close to the RADAR (<63 km) has the most pairs in the range 20–80 km. Whereas, the RADAR data far from the radar location (>63 km) has a more uniform distribution out to 150 km. This implies that the weights shift towards longer distances from (i) POINT to

(ii) close to RADAR to (iii) far from RADAR. Despite this shift, the grid points close to the RADAR still exhibit the shortest correlation distances for the long durations even compared to the POINT dataset (Fig. 9).

Another difference that can be attributed to the pseudo-CAPPI product regards spatial resolution. The spatial resolution of the radar data product is, despite the 500 m by 500 m resolution, in reality, coarser further away from the radar (as explained in Section 2.1). This might affect the correlation distances where sampled extremes span more neighbouring pixels which are sampled from the same native RADAR signal. This, in principle, creates stronger correlations between extremes at the far edges of the RADAR dataset as the weight of a group of cells, measuring the same, will be higher than for individual cells closer to the RADAR. Estimation of correlation metrics at the far RADAR range is obviously only valid in cases where there is meaningful precipitation data above the lowest beam that can be extrapolated to the ground.

The attenuation of the radar signal as a function of range is not considered a reasonable explanation since we do not see a difference in the rain intensity statistics depending on range (Fig. 8).

All in all, we can conclude that the estimated spatial correlations based on the subdivided RADAR dataset, shows a clear influence of range due to the nature of data and data processing underlying the RADAR pseudo-CAPPI product, and that the same is not the case for the intensity statistics. Since the range dependency can be caused by multiple factors, we refrain from concluding which factor, or combinations of factors, that are most plausible. We limit the conclusion of this section by acknowledging that the subdivisions of the RADAR dataset has shown substantially differences between the correlation metrics, which indicates benefits of treating the subdivided RADAR datasets separately. Generally, this emphasize the necessity of awareness to data properties, especially as function of range, for practical radar data application.

4. Conclusion

The maximum rainfall intensities and their seasonal variation are more or less in agreement for all four analyses. The re-analysis data in the coarsest resolution (RCM) is slightly underestimating the most extreme intensities for short durations, but overall structure and findings are in agreement across datasets.

The commonly used metrics for describing spatio-temporal properties are robust to the sensing method, i.e. a dense rain gauge network and radar both show the same maximum intensities across relevant durations and overall also the same correlation structure. Thus, calculating spatial correlation structures from point observations represent a fair estimate of the structure, assuming that the radar data has the "closest-to-reality" structure of the undisturbed precipitation patterns.

The study further indicates that the correlation structure derived from the RADAR data is dependent on the distance from the physical radar itself. The range dependence is a result of the nature of RADAR data and data processing and is dominant at ranges larger than 63 km. The latter has been used as a convenient measure for subdividing the RADAR data into short and long ranges from the radar. The actual range dependence is most certainly not fixed to a specific transition range (such as 63 km), but a complex range function depending on scanning routine, beam elevation, and data processing.

Despite the identified range dependence, the subdivided RADAR datasets show similar correlation length structures for the shortest durations. For longer durations the RADAR data <63 km from the radar has shorter lengths than the data >63 km from the radar, with greater agreement with the full RADAR dataset. The different correlation length structures in the subdivided RADAR dataset indicates that these datasets could be treated separately. The most important result is, however, that both observational datasets (POINT and RADAR) agree on the correlation length structure for short durations. This make it possible to conclude that the point observation used in the Danish standard method for dimensioning urban sewer systems are sufficient for describing the spatial structures for short durations. The spatial structure exhibited by the RADAR data shows that this could be a valuable addition to the point data because the spatio-temporal characteristics are so close to each other that integration should be relatively straightforward.

The study indicates that the spatial correlation lengths of high-resolution climate models (CPM) are closer to the metrics calculated on measured data than typical RCMs, but that the correlation distances for short durations are still too long, and with insufficient ability to reflect differences between different durations. Despite a clear improvement in spatial correlation structure between the convective parametrized RCM model and the convective-permitting CPM model, improvements for short duration spatial structures are still needed. However, the convective permitting models seem to represent extreme rainfall much more realistically at the event level for spatio-temporal resolutions relevant for urban hydrology. This indicates that an increasing resolution of the convective permitting CPM could solve the problems shown here in reflecting spatial differences between different resolutions. In the long-term perspective, this will decrease the need for further downscaling of climate model output, before calculation of expected climatic changes of relevance for impacts in this domain.

CRediT authorship contribution statement

Emma Dybro Thomassen: Conceptualization, Methodology, Software, Formal analysis, Writing – original draft. **Søren Liedtke Thorndahl:** Conceptualization, Methodology, Software, Formal analysis, Writing – review & editing, Supervision, Funding acquisition. **Christoffer Bang Andersen:** Software, Writing – review & editing. **Ida Bülow Gregersen:** Conceptualization, Methodology, Writing – review & editing, Funding acquisition. **Karsten Arnbjerg-Nielsen:** Conceptualization, Methodology, Writing – review & editing, Supervision, Funding acquisition. **Hjalte Jomo Danielsen Sørup:** Conceptualization, Methodology, Software, Formal analysis, Writing – original draft, Visualization, Supervision, Funding acquisition.

Declaration of Competing Interest

The authors declare that they have no known competing financial interests or personal relationships that could have appeared to influence the work reported in this paper.

Acknowledgements

Emma D. Thomassen received funding from the Danish State through the Danish Climate Atlas. All other researchers were supported by the Foundation for Development of Technology in the Danish Water Sector, Project: VÆRDI, Grant/Award Number: 57.2019. The POINT observational dataset is a product of The Water Pollution Committee of The Society of Danish Engineers made freely available for research purposes. Access to data is governed by the Danish Meteorological Institute, and they should be contacted for enquiries regarding data access. The RADAR dataset is an adjusted versions of the Danish national radar network, operated by the Danish Meteorological Institute. Aalborg University, and specifically S.L. Thorndahl, should be contacted regarding data inquires. The HCLIM simulations were performed by the NorCP (Nordic Convection Permitting Climate Projections) project group, a collaboration between the Danish Meteorological Institute (DMI), the Finnish Meteorological Institute (FMI), the Norwegian Meteorological Institute (MET Norway), and the Swedish Meteorological and Hydrological Institute (SMHI).

References

Arnbjerg-Nielsen, K., Willems, P., Olsson, J., Beecham, S., Pathirana, A., Bülow Gregersen, I., Madsen, H., Nguyen, V.-T.-V., 2013. Impacts of climate change on rainfall extremes and urban drainage systems: a review. Water Sci. Technol. 68, 16–28. https://doi.org/10.2166/wst.2013.251.

Ban, N., Caillaud, C., Coppola, E., Pichelli, E., Sobolowski, S., Adinolfi, M., Ahrens, B., Alias, A., Anders, I., Bastin, S., Belušić, D., Berthou, S., Brisson, E., Cardoso, R.M., Chan, S.C., Christensen, O.B., Fernández, J., Fita, L., Frisius, T., Gašparac, G., Giorgi, F., Goergen, K., Haugen, J.E., Hodnebrog, Ø., Kartsios, S., Katragkou, E., Kendon, E.J., Keuler, K., Lavin-Gullon, A., Lenderink, G., Leutwyler, D., Lorenz, T., Maraun, D., Mercogliano, P., Milovac, J., Panitz, H.-J., Raffa, M., Remedio, A.R., Schär, C., Soares, P.M.M., Srnec, L., Steensen, B.M., Stocchi, P., Tölle, M.H., Truhetz, H., Vergara-Temprado, J., de Vries, H., Warrach-Sagi, K., Wulfmeyer, V., Zander, M.J., 2021. The first multi-model ensemble of regional climate simulations at kilometer-scale resolution, part I: evaluation of precipitation. Clim. Dyn. 57, 275–302. https://doi.org/10.1007/s00382-021-05708-w.

Belušić, D., de Vries, H., Dobler, A., Landgren, O., Lind, P., Lindstedt, D., Pedersen, R.A., Sánchez-Perrino, J.C., Toivonen, E., van Ulft, B., Wang, F., Andrae, U., Batrak, Y., Kjellström, E., Lenderink, G., Nikulin, G., Pietikäinen, J.-P., Rodríguez-Camino, E., Samuelsson, P., van Meijgaard, E., Wu, M., 2020. HCLIM38: a flexible regional climate model applicable for different climate zones from coarse to convection-permitting scales. Geosci. Model Dev. 13, 1311–1333. https://doi.org/10.5194/gmd-13-1311-2020.

Berne, A., Delrieu, G., Creutin, J.-D., Obled, C., 2004. Temporal and spatial resolution of rainfall measurements required for urban hydrology. J. Hydrol. 299, 166–179. https://doi.org/10.1016/j.jhydrol.2004.08.002.

Ciach, G.J., Krajewski, W.F., 1999. On the estimation of radar rainfall error variance. Adv. Water Resour. 22, 585–595. https://doi.org/10.1016/S0309-1708(98)00043-8.

Cornes, R.C., van der Schrier, G., van den Besselaar, E.J.M., Jones, P.D., 2018. An ensemble version of the E-OBS temperature and precipitation data sets. J. Geophys. Res. Atmos. 123, 9391–9409. https://doi.org/10.1029/2017JD028200.

Dee, D.P., Uppala, S.M., Simmons, A.J., Berrisford, P., Poli, P., Kobayashi, S., Andrae, U., Balmaseda, M.A., Balsamo, G., Bauer, P., Bechtold, P., Beljaars, A.C.M., van de Berg, L., Bidlot, J., Bormann, N., Delsol, C., Dragani, R., Fuentes, M., Geer, A.J., Haimberger, L., Healy, S.B., Hersbach, H., Hólm, E.V., Isaksen, L., Kållberg, P., Köhler, M., Matricardi, M., Mcnally, A.P., Monge-Sanz, B.M., Morcrette, J.J., Park, B. K., Peubey, C., de Rosnay, P., Tavolato, C., Thépaut, J.N., Vitart, F., 2011. The ERA-Interim reanalysis: configuration and performance of the data assimilation system. Q. J. R. Meteorol. Soc. 137, 553–597. https://doi.org/10.1002/qj.828.

Emmanouil, S., Langousis, A., Nikolopoulos, E.I., Anagnostou, E.N., 2021. An ERA-5 Derived CONUS-wide high-resolution precipitation dataset based on a refined parametric statistical downscaling framework. Water Resour. Res. 57 https://doi.org/10.1029/2020WR029548.

Gregersen, I.B., Madsen, H., Rosbjerg, D., Arnbjerg-Nielsen, K., 2017. A regional and nonstationary model for partial duration series of extreme rainfall. Water Resour. Res. 53, 2659–2678. https://doi.org/10.1002/2016WR019554.

Gregersen, I.B., Sørup, H.J.D., Madsen, H., Rosbjerg, D., Mikkelsen, P.S., Arnbjerg-Nielsen, K., 2013. Assessing future climatic changes of rainfall extremes at small spatio-temporal scales. Clim. Change 118, 783–797. https://doi.org/10.1007/s10584-012-0669-0.

Ha, K.J., Jeon, E.H., Oh, H.M., 2007. Spatial and temporal characteristics of precipitation using an extensive network of ground gauge in the Korean Peninsula. Atmos. Res. 86, 330–339. https://doi.org/10.1016/J.ATMOSRES.2007.07.002.

Jørgensen, H.K., Rosenørn, S., Madsen, H., Mikkelsen, P.S., 1998. Quality control of rain data used for urban runoff systems. Water Sci. Technol. 37, 113–120. https://doi.org/10.2166/wst.1998.0448.

Karlsson, I.B., Sonnenborg, T.O., Refsgaard, J.C., Trolle, D., Børgesen, C.D., Olesen, J.E., Jeppesen, E., Jensen, K.H., 2016. Combined effects of climate models, hydrological model structures and land use scenarios on hydrological impacts of climate change. J. Hydrol. 535, 301–317. https://doi.org/10.1016/j.jhydrol.2016.01.069.

Kendon, E.J., Roberts, N.M., Fowler, H.J., Roberts, M.J., Chan, S.C., Senior, C.A., 2014. Heavier summer downpours with climate change revealed by weather forecast resolution model. Nat. Clim. Chang. 4, 570–576. https://doi.org/10.1038/nclimate2258.

Lind, P., Belušić, D., Christensen, O.B., Dobler, A., Kjellström, E., Landgren, O., Lindstedt, D., Matte, D., Pedersen, R.A., Toivonen, E., Wang, F., 2020. Benefits and added value of convection-permitting climate modeling over Fenno-Scandinavia. Clim. Dyn. 55, 1893–1912. https://doi.org/10.1007/s00382-020-05359-3.

Madsen, H., Arnbjerg-Nielsen, K., Mikkelsen, P.S., 2009. Update of regional intensity–duration–frequency curves in Denmark: tendency towards increased storm intensities. Atmos. Res. 92, 343–349. https://doi.org/10.1016/J.ATMOSRES.2009.01.013.

Madsen, H., Gregersen, I.B., Rosbjerg, D., Arnbjerg-Nielsen, K., 2017. Regional frequency analysis of short duration rainfall extremes using gridded daily rainfall data as covariate. Water Sci. Technol. 75, 1971–1981. https://doi.org/10.2166/wst.2017.089.

Madsen, H., Mikkelsen, P.S., Rosbjerg, D., Harremoës, P., 2002. Regional estimation of rainfall intensity-duration-frequency curves using generalized least squares regression of partial duration series statistics. Water Resour. Res. 38 (11), 21-1–21-11.

Mayer, S., Maule, C.F., Sobolowski, S., Christensen, O.B., Sørup, H.J.D., Sunyer, M.A., Arnbjerg-Nielsen, K., Barstad, I., 2015. Identifying added value in high-resolution climate simulations over Scandinavia. Tellus. Ser. A Dyn. Meteorol. Oceanogr. 67, 1–18. https://doi.org/10.3402/tellusa.v67.24941.

Médus, E., Thomassen, E.D., Belušić, D., Lind, P., Berg, P., Christensen, J.H., Christensen, O.B., Dobler, A., Kjellström, E., Olsson, J., Yang, W., 2022. Characteristics of precipitation extremes over the Nordic region: added value of convection-permitting modeling. Nat. Hazards Earth Syst. Sci. 22, 693–711. https://doi.org/10.5194/NHESS-22-693-2022.

Mikkelsen, P.S., Madsen, H., Rosbjerg, D., Harremoës, P., 1996. Properties of extreme point rainfall III: Identification of spatial inter-site correlation structure. Atmos. Res. 40, 77–98. https://doi.org/10.1016/0169-8095(95)00026-7.

Nielsen, J.E., Thorndahl, S., Rasmussen, M.R., 2014. A numerical method to generate high temporal resolution precipitation time series by combining weather radar measurements with a nowcast model. Atmos. Res. 138, 1–12. https://doi.org/10.1016/j.atmosres.2013.10.015.

Ochoa-Rodriguez, S., Wang, L.P., Gires, A., Pina, R.D., Reinoso-Rondinel, R., Bruni, G., Ichiba, A., Gaitan, S., Cristiano, E., Van Assel, J., Kroll, S., Murlà-Tuyls, D., Tisserand, B., Schertzer, D., Tchiguirinskaia, I., Onof, C., Willems, P., Ten Veldhuis, M.C., 2015. Impact of spatial and temporal resolution of rainfall inputs on urban hydrodynamic modelling outputs: A multi-catchment investigation. J. Hydrol. 531, 389–407. https://doi.org/10.1016/j.jhydrol.2015.05.035.

Olsson, J., Du, Y., An, D., Uvo, C.B., Sörensen, J., Toivonen, E., Belušić, D., Dobler, A., 2021. An analysis of (sub-)hourly rainfall in convection-permitting climate simulations over southern sweden from a user's perspective. Front. Earth Sci. 9 https://doi.org/10.3389/feart.2021.681312.

Peleg, N., Marra, F., Fatichi, S., Molnar, P., Morin, E., Sharma, A., Burlando, P., 2018. Intensification of convective rain cells at warmer temperatures observed from high-resolution weather radar data. J. Hydrometeorol. 19 (4), 715–726.

Refsgaard, J.C., 1997. Parameterisation, calibration and validation of distributed hydrological models. J. Hydrol. 198, 69–97. https://doi.org/10.1016/S0022-1694(96)03329-X.

Rosbjerg, D., Madsen, H., 2019. Initial design of urban drainage systems for extreme rainfall events using intensity–duration–area (IDA) curves and Chicago design storms (CDS). Hydrol. Sci. J. 64, 1397–1403. https://doi.org/10.1080/02626667.2019.1645958.

Schleiss, M., Olsson, J., Berg, P., Niemi, T., Kokkonen, T., Thorndahl, S., Nielsen, R., Ellerbæk Nielsen, J., Bozhinova, D., Pulkkinen, S., 2020. The accuracy of weather radar in heavy rain: a comparative study for Denmark, the Netherlands, Finland and Sweden. Hydrol. Earth Syst. Sci. 24, 3157–3188. https://doi.org/10.5194/hess-24-3157-2020.

Sørup, H.J.D., Christensen, O.B., Arnbjerg-Nielsen, K., Mikkelsen, P.S., 2016. Downscaling future precipitation extremes to urban hydrology scales using a spatio-temporal Neyman-Scott weather generator. Hydrol. Earth Syst. Sci. 20, 1387–1403. https://doi.org/10.5194/hess-20-1387-2016.

Sunyer, M.A., Sørup, H.J.D., Christensen, O.B., Madsen, H., Rosbjerg, D., Mikkelsen, P.S., Arnbjerg-Nielsen, K., 2013. On the importance of observational data properties when assessing regional climate model performance of extreme precipitation. Hydrol. Earth Syst. Sci. 17, 4323–4337. https://doi.org/10.5194/hess-17-4323-2013.

Termonia, P., Fischer, C., Bazile, E., Bouyssel, F., Brožková, R., Bénard, P., Bochenek, B., Degrauwe, D., Derková, M., El Khatib, R., Hamdi, R., Mašek, J., Pottier, P., Pristov, N., Seity, Y., Smolíková, P., Španiel, O., Tudor, M., Wang, Y., Wittmann, C., Joly, A., 2018. The ALADIN System and its canonical model configurations AROME CY41T1 and ALARO CY40T1. Geosci. Model Dev. 11, 257–281. https://doi.org/10.5194/gmd-11-257-2018.

Thomassen, E.D., Kendon, E.J., Sørup, H.J.D., Chan, S.C., Langen, P.L., Christensen, O.B., Arnbjerg-Nielsen, K., 2021. Differences in representation of extreme precipitation events in two high resolution models. Clim. Dyn. 57, 3029–3043. https://doi.org/10.1007/s00382-021-05854-1.

Thomassen, E.D., Sørup, H.J.D., Scheibel, M., Einfalt, T., Arnbjerg-Nielsen, K., 2020. Data-driven distinction between convective, frontal and mixed extreme rainfall events in radar data. Hydrol. Earth Syst. Sci. Discuss. in review. https://doi.org/10.5194/hess-2020-397.

Thorndahl, S., Einfalt, T., Willems, P., Nielsen, J.E., ten Veldhuis, M.-C., Arnbjerg-Nielsen, K., Rasmussen, M.R., Molnar, P., 2017. Weather radar rainfall data in urban hydrology. Hydrol. Earth Syst. Sci. 21, 1359–1380. https://doi.org/10.5194/hess-21-1359-2017.

Thorndahl, S., Nielsen, J., Rasmussen, M., 2019. Estimation of storm-centred areal reduction factors from radar rainfall for design in urban hydrology. Water 11, 1120. https://doi.org/10.3390/w11061120.

Thorndahl, S., Nielsen, J.E., Jensen, D.G., 2016. Urban pluvial flood prediction: a case study evaluating radar rainfall nowcasts and numerical weather prediction models as model inputs. Water Sci. Technol. 74, 2599–2610. https://doi.org/10.2166/wst.2016.474.

Thorndahl, S., Nielsen, J.E., Rasmussen, M.R., 2014. Bias adjustment and advection interpolation of long-term high resolution radar rainfall series. J. Hydrol. 508, 214–226. https://doi.org/10.1016/j.jhydrol.2013.10.056.

Vaes, G., Willems, P., Berlamont, J., 2005. Areal rainfall correction coefficients for small urban catchments. Atmos. Res. 77, 48–59. https://doi.org/10.1016/j.atmosres.2004.10.015.

Wang, L.-P., Ochoa-Rodríguez, S., Van Assel, J., Pina, R.D., Pessemier, M., Kroll, S., Willems, P., Onof, C., 2015. Enhancement of radar rainfall estimates for urban hydrology through optical flow temporal interpolation and Bayesian gauge-based adjustment. J. Hydrol. 531, 408–426. https://doi.org/10.1016/j.jhydrol.2015.05.049.

Willems, P., Vrac, M., 2011. Statistical precipitation downscaling for small-scale hydrological impact investigations of climate change. J. Hydrol. 402, 193–205. https://doi.org/10.1016/j.jhydrol.2011.02.030.